stable cation arrangements to be produced in both cases. Tables 2 and 5 show that there are few cation–cation distances comparable to the $d(M–M)$ values used in the restrained refinements of the starting models. Although O^{2-} has a greater ionic radius than La^{3+} or Pd^{2+}, the minimum O–O distance in these materials is less than the smallest cation–cation distance, reflecting the greater polarizability of the anion. Thus, it is more useful to consider cation–cation distances than anion–anion contacts in attempting to model such structures.

The author thanks W. T. A. Harrison and W. I. F. David for assistance with the collection and analysis of HRPD data, D. J. Watkin for help with *CRYSTALS* and many useful discussions, and Christ Church, Oxford, for a Junior Research Fellowship. The palladium oxide used in this work was kindly supplied by Johnson Matthey Chemicals.

References

ATTFIELD, J. P. & FEREY, G. (1988). *J. Solid State Chem.* Submitted.

ATTFIELD, J. P., SLEIGHT, A. W. & CHEETHAM, A. K. (1986). *Nature (London)*, **322**, 620–622.

BACON, G. E. (1975). *Neutron Diffraction*, 3rd ed. Oxford: Clarendon Press.

BROWN, P. J. & MATTHEWMAN, J. C. (1987). *The Cambridge Crystallography Subroutine Library – Mark 3 User's Manual.* Report No. 87-010. Rutherford–Appleton Laboratory, Didcot, England.

CHEETHAM, A. K. (1988). In *Chemical Crystallography with Pulsed Neutrons and Synchrotron X-rays*, edited by M. A. CARRONDO & G. A. JEFFREY, pp. 137–158. Kluwer Academic Publishers, Dordrecht.

CHEETHAM, A. K., DAVID, W. I. F., EDDY, M. M., JAKEMAN, R. J. B., JOHNSON, M. W. & TORARDI, C. C. (1986). *Nature (London)*, **320**, 46–48.

COX, D. E., HASTINGS, J. B., CARDOSO, L. P. & FINGER, L. W. (1986). *Mater. Sci. Forum*, **9**, 1–20.

COX, D. E., HASTINGS, J. B., THOMLINSON, W. & PREWITT, C. (1983). *Nucl. Instrum. Methods*, **208**, 573–578.

HENDRICKSON, W. A. & KONNERT, J. H. (1980). In *Computing in Crystallography*, edited by R. DIAMOND, S. RAMASESHAN & K. VENKATESAN, pp. 13.01–13.26. Bangalore: Indian Academy of Sciences.

International Tables for X-ray Crystallography (1974). Vol. IV. Birmingham: Kynoch Press. (Present distributor Kluwer Academic Publishers, Dordrecht.)

JOHNSON, M. W. & DAVID, W. I. F. (1985). Report No. 85-112. Rutherford–Appleton Laboratory, Didcot, England.

KAKHAN, B. G., LAZAREV, V. B. & SHAPLYGIN, I. S. (1982*a*). *Russ. J. Inorg. Chem.* **27**, 1180–1182.

KAKHAN, B. G., LAZAREV, V. B. & SHAPLYGIN, I. S. (1982*b*). *Russ. J. Inorg. Chem.* **27**, 2395–2401.

LEHMANN, M. S., CHRISTENSEN, A. N., FJELLVAG, H., FEIDENHANS'L, R. & NIELSEN, M. (1987). *J. Appl. Cryst.* **20**, 123–129.

MCDANIEL, C. L. & SCHNEIDER, S. J. (1968). *J. Res. Natl Bur. Stand. Sect. A*, **72**(1), 27–37.

MAICHLE, J. K., IHRINGER, J. & PRANDL, W. (1988). *J. Appl. Cryst.* **21**, 22–27.

RIETVELD, H. M. (1969). *J. Appl. Cryst.* **2**, 65–71.

ROLLETT, J. S. (1969). In *Crystallographic Computing*, edited by F. R. AHMED, pp. 167–182. Copenhagen: Munksgaard.

SHANNON, R. D. (1976). *Acta Cryst.* A**32**, 751–767.

VISSER, J. W. (1969). *J. Appl. Cryst.* **2**, 89–95.

WATKIN, D. W. (1988). In *Crystallographic Computing* 4, edited by N. W. ISAACS & M. R. TAYLOR. International Union of Crystallography/Oxford Univ. Press.

WATKIN, D. W., CARRUTHERS, J. R. & BETTERIDGE, P. W. (1985). *CRYSTALS User Guide.* Chemical Crystallography Laboratory, Univ. of Oxford, England.

WISEMAN, P. (1974). DPhil Thesis, Univ. of Oxford, England.

YVON, K., JEITSCHKO, W. & PARTHÉ, E. (1977). *J. Appl. Cryst.* **10**, 73–74.

Acta Cryst. (1988). B**44**, 568–575

Examination of *n*-Beam Interaction: X-ray Experiment and Simulation for $KMnF_3$

BY A. OKAZAKI, Y. SOEJIMA, M. MACHIDA* AND H. OHE†

Department of Physics, Kyushu University, Fukuoka 812, *Japan*

(*Received* 25 *February* 1988; *accepted* 27 *June* 1988)

Abstract

The intensity equation of the *n*-beam interaction based on the kinematical theory [Soejima, Okazaki & Matsumoto (1985). *Acta Cryst.* A**41**, 128–133] is examined for the case of X-ray diffraction in $KMnF_3$. With a few examples of the fundamental and superlattice diffractions, it is shown that the equation reproduces the experimental ψ-scan patterns which result from *n*-beam interaction. The spectral width of the incident beams is the main contribution to the thickness of the Ewald sphere, and is taken into account. It is confirmed that the ψ-scan patterns are sensitive to the symmetry of the crystal structure: the patterns must be and are identical for symmetry-equivalent reflections, and vary at the structural phase transition with a change in symmetry.

* Present address: The Research Reactor Institute, Kyoto University, Kumatori-cho, Osaka 590-04, Japan.

† Present address: Tsukuba Research Laboratories, Eisai Co. Ltd, Tsukuba, Ibaraki 300-26, Japan.

0108-7681/88/060568-08$03.00

Introduction

The effect of n-beam interaction (multiple diffraction) on X-ray or neutron diffraction has been extensively studied since Renninger (1937) first observed the *Umweganregung*. There are two branches of this field. One is based on the dynamical theory and concerned with the phase problem (*e.g.* Chang, 1984). The other is, in contrast, based on the kinematical theory, and mainly related to the correction of the intensity data for structure determination. The papers by Tanaka & Saito (1975) and LePage & Gabe (1979), both following the intensity equation given by Moon & Shull (1964), are examples of the second branch. Overall effects on the intensity data and consequently on the structure determination are examined. Another example is the work by Soejima, Okazaki & Matsumoto (1985) (SOM); an intensity equation, derived on the basis of the kinematical theory, is used for simulation of a ψ scan, a scan about the scattering vector, and compared with experiment with four-circle diffractometers. The analysis shows the contribution of individual n-beam interactions. We can therefore examine the detail of the phenomenon. Although experimental ψ-scan patterns in the literature were limited, fair agreement was observed. Recent installation of an Enraf–Nonius CAD-4 diffractometer at Kyushu University made it possible for the present authors to make a full examination of the SOM formalism and the n-beam interaction itself.

In the present paper, a comparison of ψ-scan patterns will be made between calculation and experiment for a series of reflections. As the n-beam interaction is a higher-order phenomenon, the measurement of the effect on the intensity may be seriously disturbed by the statistical fluctuation of the intensity. For this reason, it is not appropriate to quantify the comparison in a manner like that used in the Rietveld analysis of the powder diffraction pattern; instead, we choose a visual qualitative comparison of the patterns as the best procedure. In the following, $KMnF_3$ with a perovskite structure is the test material. Since the crystal has a superlattice structure below the cubic-to-tetragonal transition at $T_c = 186{\cdot}6$ K, we can use the reflections of both fundamental and superlattice structures with a wide range of intensities. The indexing of crystallographic quantities for both the cubic and tetragonal phases will be based on the unit cell of the superlattice structure. Two indexing schemes will be used: one is based on the unit cell of size $2a \times 2a \times 2c$ and the other on $2^{1/2}a \times 2^{1/2}a \times 2c$, where $a \simeq c \simeq 4$ Å. The indices based on the former and the latter will be given without and with the subscript t, respectively. The space group $I4/mcm$ in the tetragonal phase is relevant to the latter. For convenience we mainly use the former scheme; we then have hkl all even or all odd for the fundamental and superlattice reflections, respectively. Among the former, $h + k + l = 4n$ and $h + k + l = 4n \pm 2$ generally specify strong and weak fundamental reflections, respectively.

Calculations

Soejima *et al.* (1985) showed that the effect of the n-beam interaction on the intensity at the reciprocal-lattice point $\mathbf{h}$ can be described, owing to a small value of the reflectivity, by summing the effects of independent three-beam interactions (the double diffractions):

$$(I_{\mathbf{h}})_{\rm obs}/rI_0 = N_{\mathbf{h}}\{1 - r(\textstyle\sum_i N_{{\rm op}i} + \sum_i N_{{\rm co}i})\} + r\textstyle\sum_i N_{{\rm op}i} N_{{\rm co}i}, \quad (1)$$

where I_0 denotes the incident intensity and r the effective reflectivity including absorption and extinction. It is assumed that the value of r is the same for different reflections, while the $N_{\mathbf{h}}$ are normalized to the largest of them.

$$N_{\mathbf{h}} = |F_h|^2 {\rm Lp}. \quad (2)$$

On the right-hand side, conventional notation is used. The subscripts op and co indicate the operative and cooperative points, respectively. The coordinates of these points will be given by $\mathbf{h}_{\rm op}$ and $\mathbf{h}_{\rm co}$, respectively, which are related to each other by the relation

$$\mathbf{h} = \mathbf{h}_{\rm op} + \mathbf{h}_{\rm co}. \quad (3)$$

The L and p factors for three-beam cases given respectively by Post (1975) and Zachariasen (1965) are used; for the p factor, details have been given by Soejima *et al.* (1985).

As schematically shown in Fig. 1, the actual Ewald sphere has a finite non-uniform thickness arising from (*a*) the spectral width $\Delta\lambda$ and (*b*) the divergence $\Delta\omega$ of the incident beams. If we neglect the operative points with large $|h_{\rm op}|$, which are, for example, above the dotted line in the figure, the effect of $\Delta\lambda$ and $\Delta\omega$ can be described roughly by one parameter $\Delta\lambda/\lambda$. In the case of X-rays with shorter wavelengths like Mo $K\alpha$, the condition will be satisfied to a fair approximation; this is in accordance with experience (Soejima *et al.*, 1985).

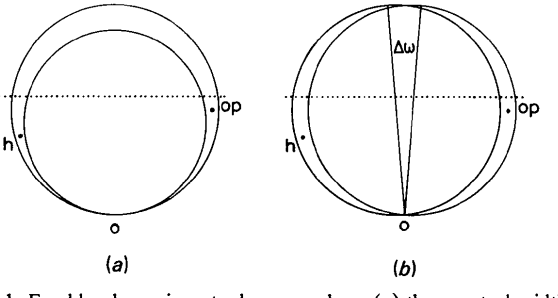

Fig. 1. Ewald spheres in actual cases, where (*a*) the spectral width $\Delta\lambda$ and (*b*) the divergence $\Delta\omega$ bring about non-uniform thickness. The effects are exaggerated. The radii of the two circles in (*a*) are $1/(\lambda - \Delta\lambda)$ and $1/(\lambda + \Delta\lambda)$.

The value of $\Delta\lambda/\lambda = 0{\cdot}01$ is empirically chosen; it will be shown below that this value is consistent with the instrumental resolution. A more quantitative discussion will be given in the last section.

In the calculation we place the point **h** in the middle of the thickness of the actual Ewald sphere; the summation in (1) will then be made for $\mathbf{h}_{op}$ in the thickness. To make the calculating time shorter, a quicker search of relevant $\mathbf{h}_{op}$ is essential. From the original intensity data file, a new file which consists of pairs of $\mathbf{h}_{op}$ and $\mathbf{h}_{co}$ following (3) is prepared for each **h**, and used for the calculation of (1). In the present paper, the intensity data used are those experimentally determined, but they can also be obtained from the structure parameters.

Experiment

Measurements were made on the CAD-4 diffractometer with graphite (002) monochromatized Mo $K\alpha$ radiation; the p factor of the monochromator ($\theta = 6{\cdot}1°$) can be approximated to 1, and will not affect the p factor of the n-beam interaction in the specimen. A PDP 11/23 computer is used for controlling the diffractometer and for the calculations mentioned above. The specimen prepared from a flux-grown crystal is a sphere 0·3 mm in diameter and sealed in a glass capillary. Two series of measurements were made at 156 and 300 K with a stability better than 1 K; an Enraf–Nonius low-temperature attachment was used. The intensity data for the simulation of the ψ scans were collected, with $\omega/2\theta$ scans in one octant of the reciprocal lattice; the numbers of reflections surveyed in the region $\theta = 2$–$32°$ are 298 and 177 at 156 and 300 K, respectively. The data for the other octants were also required for the simulation, and prepared from the data mentioned above by assuming the symmetry equivalence. For several **h**, the ψ scan was made in steps of 0·05 or 0·1°; the intensity at each ψ position being determined from $\omega/2\theta$ scans.

Below T_c, $KMnF_3$ usually shows domain structures; a single peak of diffraction in the cubic phase will then show a splitting. In the present case, however, we observed no splitting but only a slight broadening of the peaks. Therefore, the orientation matrix (the **UB** matrix) at 156 K is determined on the basis of a cubic lattice. The value of c/a is about 1·004 at 156 K (Kawaminami & Okazaki, unpublished). This is a measure of the resolution of the diffractometer, and is consistent with an empirical choice of the value of $\Delta\lambda/\lambda = 0{\cdot}01$ mentioned above.

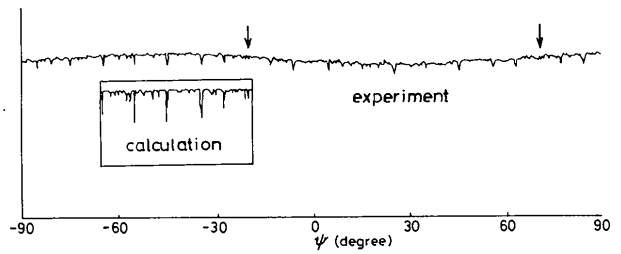

Fig. 2. ψ-scan pattern for 400, the strongest reflection; the symmetry points are marked with arrows. As expected from equation (1), only dips are observed on the base line; the sinusoidal variation of the base line is due to anisotropy of the absorption. The inset shows a calculated pattern expanded vertically.

Comparison of calculation with experiment

If we rewrite (3) in the form

$$\begin{bmatrix} h \\ k \\ l \end{bmatrix}_{\mathbf{h}} = \begin{bmatrix} h \\ k \\ l \end{bmatrix}_{op} + \begin{bmatrix} h \\ k \\ l \end{bmatrix}_{co}, \qquad (4)$$

we obtain the following relation between hkl's of the operative (op) and cooperative (co) points. For the fundamental **h** points, with hkl all even, the op and co points must be both fundamental or both superlattice points. For the superlattice **h** points, on the other hand, the op and co points must be pairs of fundamental and superlattice points. Comparisons of simulation with experiment have been made for the **h** points as follows: 200, 400, 600, 266, 10,0,0, 2,2,10, 0,6,10, 2,6,10, 6,6,10, 111, 113, 331, 333, 553 and 555. Some examples will be shown in the following.

In Fig. 2 the experimental pattern of the ψ scan is shown for 400, the strongest reflection, with an intensity $I = 10^3$ on an arbitrary but common scale. As seen from (1), the intensity of the n-beam interaction for the strongest **h** cannot be positive. The ψ-scan pattern therefore shows some dips; this is in agreement with observation. A sinusoidal fluctuation of the base line can be attributed to anisotropic absorption by the capillary and/or the slightly aspherical specimen. The arrows indicate the symmetry points of the pattern. The inset shows a calculated pattern. Although the statistical fluctuation of a few percent of the intensity has smeared the detail of the experimental curve, an overall agreement between calculation and experiment is obvious.

In Fig. 3, the calculated pattern for 400 is shown on an expanded scale. The assignments of hkl's of the op and co points are given for some dips; $h + k + l$ is $4n$ for both op and co points. Although a combination of weak op and co points with $h + k + l = 4n \pm 2$ is mathematically allowed, the effect is usually negligible, as seen from (1). We also see from (1) that the dip is more pronounced when op and co points are of large intensities with small hkl's. The dip assigned by six pairs of op and co points is an example of the eight-beam case; the calculation is made for the six independent three-beam cases.

Fig. 4 shows the comparison for the fundamental 600 with a weak intensity $I = 3{\cdot}6$. In this case, owing to the

weak intensity, the statistical fluctuation smeared most features of the n-beam interaction of the experimental curve (a). The discussion below can be confirmed by only a few definite peaks and dips. Here, $h + k + l$ is $4n$ for one of the op and co points and $4n \pm 2$ for the other. Since the intensity of the latter is much weaker than that of the former, it will be a reasonable approximation to neglect one of the terms in parentheses on the right-hand side of (1). In the ψ-scan pattern, we therefore get a peak when both op and co are stronger than 600, while we find a dip when either op or co is weaker than 600. This is in agreement with observation; the intensity values used for the calculation are given in parentheses after the relevant hkl values.

The case of 2,10,2, the weakest fundamental reflection with $I = 0{\cdot}5$, is shown in Fig. 5. It is obvious from (1) that we only observe peaks above the base line. As in the case of 600, $h + k + l$ is $4n \pm 2$ for an op or co point; if that is of large intensity, like 200, 222 or 420, we find a large peak.

In the following, superlattice **h** reflections are examined. Fig. 6 shows the calculated and observed patterns of 313 with $I = 2{\cdot}0$, the third strongest of the superlattice reflections. In spite of the poor signal/noise (S/N) ratio in the observed pattern, the following observations can be made. The strongest superlattice reflection is 113 and the second is 335; $I = 3{\cdot}8$ and $2{\cdot}2$, respectively. Since the op and co points are a pair of the fundamental and superlattice reflections, and since 113 is the only superlattice reflection significantly stronger than 331, all the peaks are due to the combination of 113 and one strong fundamental reflection. This is why the number of peaks with significant intensity is small. It is also readily derived from (1) that, when weakest or zero-intensity superlattice reflections, in particular those of space-group extinctions, are included, we get remarkable dips: 111 and 333 respectively correspond to 011_t and 033_p which are absent owing to the **c** glide, and for 713 $I = 0{\cdot}5$.* It is therefore obvious that, for the simulation of the dips, reflections of zero or very weak intensities must be included in the intensity data set. The situation is in contrast to the case of 400, where

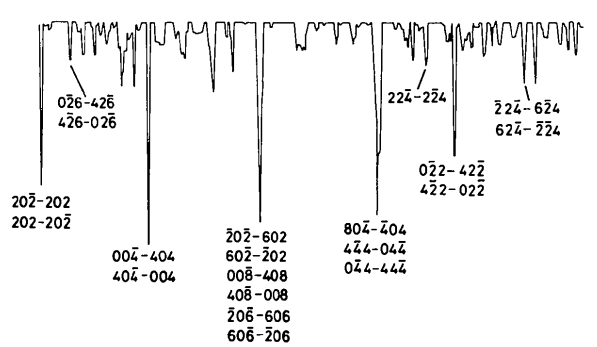

Fig. 3. Calculated ψ-scan pattern for 400; assignments of op and co points are given for some dips.

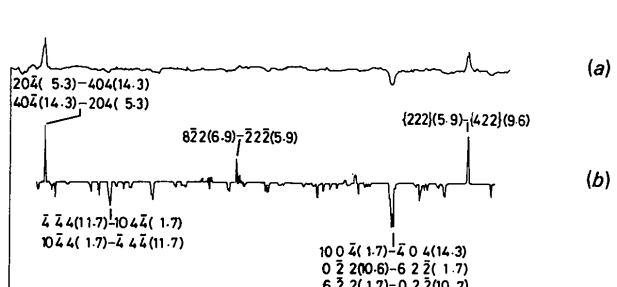

Fig. 4. Comparison of (a) experiment and (b) calculation of ψ scanning for 600; the pattern in (b) is vertically expanded and vertically shifted. Assignments of op and co points with relevant intensities in parentheses are given for some peaks and dips. There are four symmetry-equivalent sets contributing to the peak marked as {222}–{422}.

* In more quantitative discussions, one must take account of the domain structure as shown by Okazaki & Ono (1978) and Okazaki, Soejima & Machida (1987).

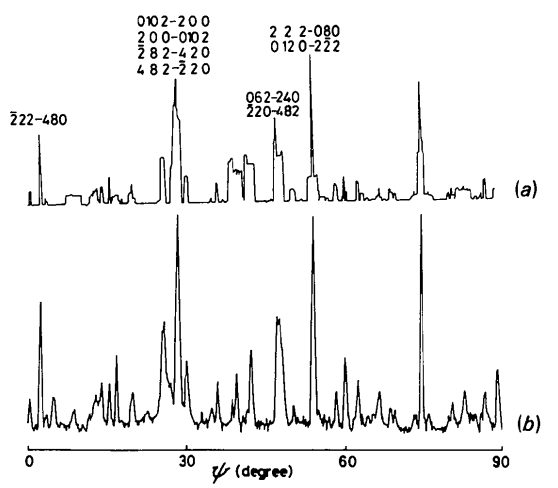

Fig. 5. Comparison of (a) calculation and (b) experiment of ψ scanning for 2,10,2.

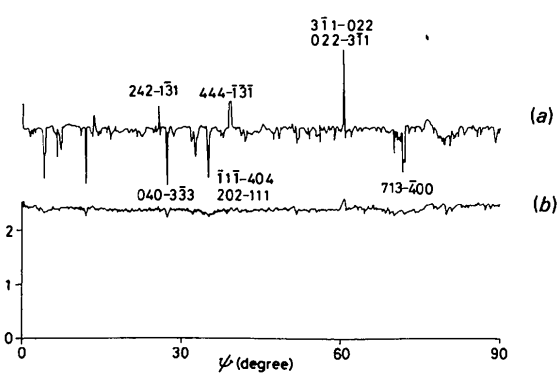

Fig. 6. ψ-scan patterns for the superlattice diffraction 313: (a) calculation and (b) experiment. In (a), the pattern is vertically expanded.

the combination of strong op and strong co points brings about distinct dips. The experimental curve for 313 has an S/N ratio even poorer than that for 600. It is therefore remarkable that the recognizable peaks and dips can still be assigned in a way which is consistent with (1).

In Fig. 7, the case of 333 is shown. Since $I = 0$ for this case, the observed pattern is not disturbed by the fluctuation of the base line; this is therefore a good example to show to what degree the calculation can reproduce the detail of the observed pattern. Since $N_{\mathbf{h}} = 0$ in (1), only the last term, *Umweganregung* (Renninger, 1937), contributes to the intensity. A combination of a strong fundamental point and a strong superlattice one gives rise to a large peak. For the cases including superlattice points 351 and 117, with medium intensities 1·6 and 1·1, respectively, the peaks are medium or small.

It is to be noted that there is a slight deviation from symmetry about the mirror point in the pattern marked by an arrow. The deviation is more significant in the calculated pattern; the peaks numbered 1, 2 and 3 are weaker than those at the symmetry-related positions. This fact is due to the finite thickness of the Ewald sphere shown in Fig. 1. Let us consider case (*a*). If the op point is on a sphere relevant to the wavelength λ on which we find the **h** point, we obtain a symmetrical pair of peaks. As shown in Fig. 7 by the assignment of op and co points for the largest pair of the peaks, the op and co points are interchanged for the corresponding peaks.

In Fig. 8, a schematic illustration is given for the situation which results in the deviation from symmetry; the op and co points at the second ψ position are respectively equivalent to the co and op points at the first ψ position, and are specified by primes. If the op point is not in the middle of the sphere while the **h** point is, the op′ point may appear outside the actual Ewald sphere. The contribution of the op′–co′ pair is then lost, effecting asymmetry. This will happen more frequently for the co, and therefore the op′ vectors of shorter lengths, because the actual Ewald sphere is thinner near the origin. This is consistent with the observations in Fig. 7. The missing contributions to the peaks 1, 2 and 3 are those from the pairs $0\bar{2}0$–353, 020–313 and $\bar{2}\bar{2}0$–553, respectively; 020 and 220 are respectively the nearest and the second nearest to the origin. The deviation from symmetry in the calculated pattern is more prominent than that in the observed one. This can be attributed to an inaccurate choice of the parameter $\Delta\lambda/\lambda$, and to neglect of the effect of beam divergence; the effect will be mentioned in the last section. A deviation from symmetry is also found in the width of the peak; the largest pair of peaks mentioned above is an example. In addition to the low background, the high symmetry about the ψ axis makes the present discussion unambiguous.

Further ψ-scan measurements are made for 343, which is not allowed by the lattice type. As pointed out by Lipson & Cochran (1953), there will be no *n*-beam interaction in this case; only random fluctuations of the background are observed.

Symmetry

The ψ-scan pattern is directly related to the symmetry of the structure. The patterns for the symmetry-equivalent diffractions therefore must be the same (Okazaki, Ohe & Soejima, 1988). Fig. 9 shows two sets of patterns for (*a*) 10,2,2, 2,10,2 and 2,2,10 and (*b*) 2,6,10, 6,2,10 and 10,6,2 all taken at 300 K; for (*b*), the three other symmetry-equivalent points 6,10,2 *etc.* also show the same order of agreement of the patterns. The results, including those for a few other symmetry-equivalent sets of reflections, indicate the reliability of the experimental system and, at the same time, confirm the cubic symmetry of the specimen crystal at this temperature.

The ψ value in the diffractometer coordinates used in the measurement does not necessarily coincide with

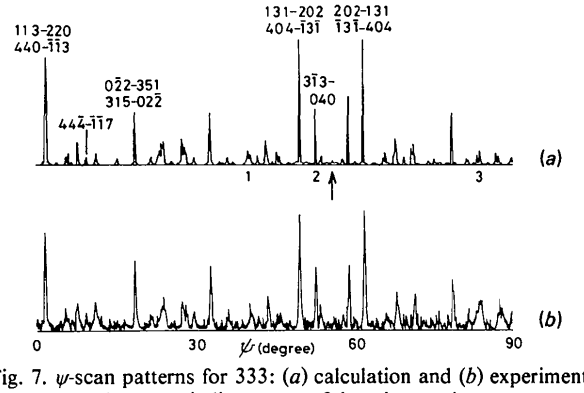

Fig. 7. ψ-scan patterns for 333: (*a*) calculation and (*b*) experiment. The arrow indicates one of the mirror points.

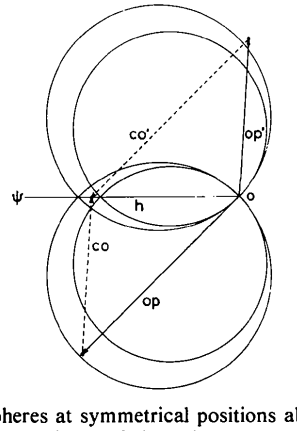

Fig. 8. Ewald spheres at symmetrical positions about the ψ axis. If op is not in the middle of the sphere, op′ can be outside the corresponding sphere.

that in the crystal coordinates. For example, the origin of the ψ coordinate in the CAD-4 system is chosen as a position which gives a minimum value of χ for the relevant reflection; the conventional intensity measurement is made at this ψ position. Therefore, the measurements for equivalent reflections are not made, in general, at equivalent ψ positions. In Fig. 9, the patterns of each set are arranged on a common ψ coordinate. Tanaka & Saito (1975) have mentioned that non-equal intensities between equivalent reflections are partly due to the *n*-beam effect; the description is not correct, and should read, instead, due to a difference in the *n*-beam effect at non-equivalent ψ positions. A typical example of such non-equal intensities is shown by Okazaki *et al.* (1988) for 001 of Nb_3Sn.

As is well known, the widths of the *n*-beam diffraction extrema are narrower than those of the profiles of the primary diffracted intensities. This suggests that we may find the effect of the tetragonal distortion of the unit cell on the ψ-scan pattern even though we cannot find the peak splitting in the conventional $\omega/2\theta$ scan. Fig. 10 shows a series of the ψ-scan patterns of 2,10,2 above and below the transition temperature; since the transition is weakly first order, some abrupt changes in the relative intensity and in the profile of the peaks are obvious when the temperature varies through the transition at 186·6 K. The patterns for 10,2,2, 2,10,2 and 2,2,10 taken at 156 K showed that these reflections were no longer equivalent, and suggested that the domain distribution could be determined by analysing the difference of the peak profiles of these patterns.

A change in the crystal symmetry or a resulting split of an X-ray diffraction peak can be determined more accurately by means of a sophisticated technique like the double-crystal diffraction method (Okazaki, Soejima, Ohama & Müller, 1985). What is to be noted here is that the ψ scan can be made on a four-circle diffractometer without remounting a specimen crystal used for the intensity data collection. While we cannot conclude that there is a change in symmetry, as in the present case, from the peak broadening observed in the $\omega/2\theta$ scan, we can do it, practically and reliably, observing equivalence or non-equivalence of relevant ψ-scan patterns.

Discussion

As shown in the previous section, the SOM formalism of the *n*-beam interaction reproduces observed ψ-scan patterns. This is also the case not only for all the other reflections of $KMnF_3$ but also for other crystals; some examples for Nb_3Sn are reported elsewhere (Okazaki *et al.*, 1988). An application has also been made to neutron diffraction (Soejima *et al.*, 1985).

Let us examine the reasons why the agreement between the calculation and experiment of ψ scanning is satisfactory. Firstly, the use of the kinematical theory; this is applicable to mosaic crystals, in which the size of the mosaic domains is smaller than the extinction length. Most specimens for X-ray diffraction, in particular those for structure determination on the four-circle diffractometer, belong to this category.

Secondly, the parameters $\Delta\lambda/\lambda$ and $\Delta\omega$. As seen in Fig. 1, the θ dependences of the thickness of the Ewald spheres in (*a*) and (*b*) are quite different. The situation is compared in Fig. 11, where the curves (*a*) and (*b*)

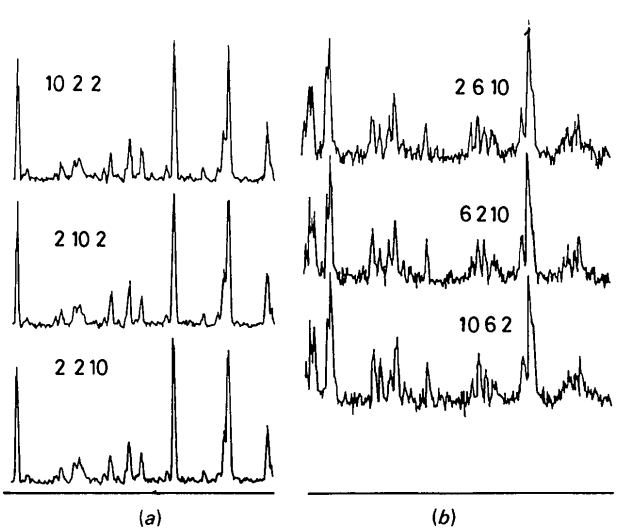

Fig. 9. ψ-scan patterns observed at symmetry-equivalent points for (*a*) 10,2,2, 2,10,2 and 2,2,10 and (*b*) 2,6,10, 6,2,10 and 10,6,2.

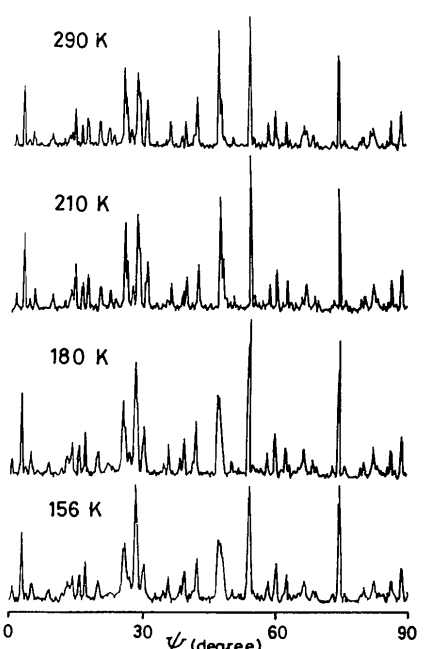

Fig. 10. ψ-scan patterns for 2,10,2 above and below the transition temperature 186·6 K.

respectively correspond to the cases (a) and (b) in Fig. 1. The curves are given by the following equations.

For (a),

$$\Delta l/(1/\lambda) = l_1 - l_2, \tag{5}$$

where

$$l_1^2 = (1+\Delta)^2+\Delta^2-2\Delta[\Delta\sin^2 2\theta - (1+2\Delta+\Delta^2\cos^2 2\theta)^{1/2}\cos 2\theta],$$

$$l_2^2 = (1-\Delta)^2+\Delta^2-2\Delta[\Delta\sin^2 2\theta + (1-2\Delta+\Delta^2\cos^2 2\theta)^{1/2}\cos 2\theta]$$

and

$$\Delta = [(\lambda-\Delta\lambda)^{-1}-(\lambda+\Delta\lambda)^{-1}]/2.$$

For (b)

$$\Delta l/(1/\lambda) = 2\sin(\Delta\omega/2)\sin 2\theta - [4\sin^2(\Delta\omega/4)\sin^2(2\theta+\Delta\omega/4) - 4\sin^2(\Delta\omega/4)+1]^{1/2} + [4\sin^2(\Delta\omega/4)\sin^2(2\theta-\Delta\omega/4) - 4\sin^2(\Delta\omega/4)+1]^{1/2}. \tag{6}$$

The notation is defined in Figs. 1 and 11. The parameters used are $\Delta\lambda/\lambda = 0{\cdot}01$ and $\Delta\omega = 0{\cdot}2°$, which are appropriate for the present experimental conditions. The success of the calculation here results from the fact that $\Delta\lambda/\lambda$ is essential in determining the effective thickness of the Ewald sphere. In a better approximation, however, the thickness corresponds to the envelope of the two curves, which describes a more real Ewald sphere. Therefore we may have lost some op points in the region related to the area shown hatched in Fig. 11. As mentioned in the explanation of Fig. 7, the discrepancies between the calculated and observed patterns are attributed to the exclusion of 020 and 220 as the op points in the calculation. The 2θ values of these points are 20 and 28° respectively; they are therefore in the area mentioned above. In the present formalism, it is confirmed that the discrepancy disappears if we take $\Delta\lambda/\lambda = 0{\cdot}02$; this fact is consistent with the present discussions.

Thirdly, a nearly constant value of reflectivity r for all the diffraction of $KMnF_3$. The r values can be determined from the comparison of the observed and calculated ratios of the intensity due to the n-beam interaction to that of its own. The values thus obtained range from 0·4 to 0·5% for all the cases.* This encourages us to take a constant r value in the calculation of the n-beam effect.

It is therefore confirmed that the assumptions made in the calculation are reasonable; this is the reason for the good agreement. Further improvement will be attained when we take account of the effect of the beam divergence and crystal mosaicity on the thickness of the Ewald sphere. A modification of the program is also necessary when the effect of the anomalous dispersion is significant.

In the conventional structure analysis, the effect of n-beam interaction is not explicitly taken into account. Since the effect reaches 10% of the original intensity for strong reflections, and more for weak ones, we must be careful when a detailed determination of the electron density distribution is concerned. Tanaka & Saito (1975), LePage & Gabe (1979) and Hauback & Mo (1988) have made, in a systematic way, a correction for the n-beam effect in structure analysis. The effective Ewald spheres considered there, however, are those of homogeneous thickness (Tanaka, private communication; Mo, private communication). Soejima *et al.* (1985) found that this is a poor approximation which introduces an excess thickness near the origin of the reciprocal space. An over-counting of the op points in that region is more serious in the case of X-ray diffraction because of larger f values there. As expected, the approximation is hardly acceptable to the simulation of the ψ scan because the pattern is sensitive to individual n-beam interactions. In the structure determination, in contrast, we measure the integrated intensity only at $\psi = 0$. The effect of the n-beam interaction on that particular intensity is generally small; the correction for the n-beam effect is therefore not very sensitive to the approximation. Nevertheless, if we need the correction, the calculation should be based on a best approximation for the real Ewald sphere.

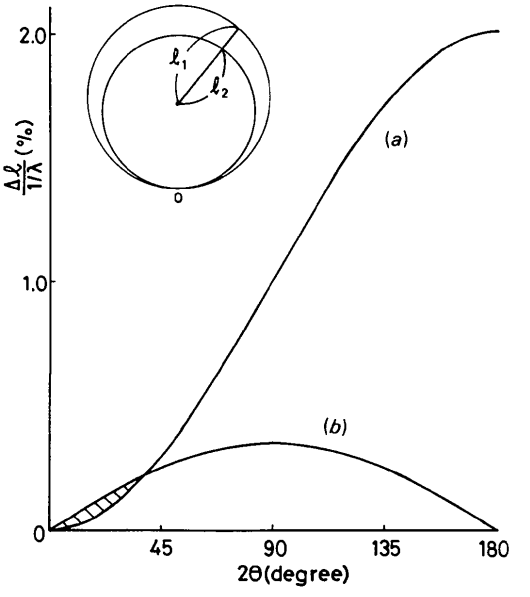

Fig. 11. Thickness of Ewald sphere as a function of the scattering angle 2θ. The parameters chosen are $\Delta\lambda/\lambda = 0{\cdot}01$ for (a), and $\Delta\omega = 0{\cdot}2°$ for (b).

* If the intensity is zero as in the case of 333, or if it is very weak, we cannot determine the r value in this way. For 220 of Nb_3Sn, on the other hand, we found $r = 2\%$ (Okazaki *et al.*, 1988).

The n-beam interaction brings about highly resolved ψ-scan patterns. Through this fact, we can get accurate information on the symmetry equivalence of a set of reflections and on a change in the symmetry at a structural phase transition. The high resolution is, at the same time, advantageous in checking the reliability of the goniometer and other parts of the diffractometer.

The experiment and simulation were carried out at the Centre of Advanced Instrumental Analysis, Kyushu University. The authors are indebted to Dr Y. Suemune for growing the crystal. One of the authors (AO) is grateful to Professor M. Renninger for encouragement and comments which have been given since the beginning of a series of studies on n-beam interaction, and to Dr K. Tanaka and Professor F. Mo for stimulating discussions at the International Symposium on Accuracy in Structure Factor Measurement (Warburton, Australia, 1987).

References

CHANG, S. L. (1984). *Multiple Diffraction of X-rays in Crystals*, ch. 7. Berlin: Springer.
HAUBACK, B. C. & MO, F. (1988). *Aust. J. Phys.* In the press.
LEPAGE, Y. & GABE, E. J. (1979). *Acta Cryst.* A**35**, 73–78.
LIPSON, H. & COCHRAN, W. (1953). *The Determination of Crystal Structure*, p. 32. New York: Cornell Univ. Press.
MOON, R. M. & SHULL, C. G. (1964). *Acta Cryst.* **17**, 805–812.
OKAZAKI, A., OHE, H. & SOEJIMA, Y. (1988). *Aust. J. Phys.* In the press.
OKAZAKI, A. & ONO, M. (1978). *J. Phys. Soc. Jpn*, **45**, 206–211.
OKAZAKI, A., SOEJIMA, Y. & MACHIDA, M. (1987). *J. Phys. C*, **20**, 1041–1045.
OKAZAKI, A., SOEJIMA, Y., OHAMA, N. & MÜLLER, K. A. (1985). *Jpn J. Appl. Phys.* **S24-2**, 257–259.
POST, B. (1975). *J. Appl. Cryst.* **8**, 452–456.
RENNINGER, M. (1937). *Z. Phys.* **106**, 141–176.
SOEJIMA, Y., OKAZAKI, A. & MATSUMOTO, T. (1985). *Acta Cryst.* A**41**, 128–133.
TANAKA, K. & SAITO, Y. (1975). *Acta Cryst.* A**31**, 841–845.
ZACHARIASEN, W. H. (1965). *Acta Cryst.* **18**, 705–710.

Acta Cryst. (1988). B**44**, 575–580

Structure of Barium Plutonate by Neutron Powder Diffraction

BY GARY G. CHRISTOPH,* ALLEN C. LARSON,† P. GARY ELLER,‡ JOHN D. PURSON,‡ JOHN D. ZAHRT,§ R. A. PENNEMAN‡ AND GARY H. RINEHART¶

Los Alamos National Laboratory, University of California, Los Alamos, NM 87545, *USA*

(*Received* 10 *March* 1988; *accepted* 26 *July* 1988)

Abstract

The three-dimensional crystal structure of barium plutonate, $BaPuO_3$, has been determined using Rietveld refinement of room-temperature time-of-flight neutron powder diffraction data obtained with the prototype neutron powder diffractometer (NPD) at the Los Alamos pulsed neutron facility (LANSCE). A distorted perovskite structure ($GdFeO_3$ type) is found which contains nearly regular PuO_6 octahedra with Pu—O distances of 2·2306 (5), 2·2295 (12) and 2·2230 (12) Å and unique *cis* O—Pu—O angles of 88·58 (2), 89·26 (7) and 89·59 (7)°. The PuO_6 octahedra are rotated to give Pu—O—Pu angles of 157·07 (8) and 160·53 (5)°, as compared with 180° in cubic perovskites. The observed Pu—O distances and the deviations from the cubic perovskite structure are in excellent accord with expectations based on crystal chemical models. Crystal data: $BaPuO_3$, $M_r = 427·3$, orthorhombic, *Pbnm*, $a = 6·219$ (1), $b = 6·193$ (1), $c = 8·744$ (1) Å, $V = 336·8$ Å^3, $Z = 4$. The final integrated reflection $R(F^2)$ factor is 0·034 for all reflection data from three independent detector banks. The NPD instrument and its characteristics are described.

Introduction

A large number of ABO_3 oxides adopt a structure closely related to the perovskite structure type. In the past, such materials have been investigated intensively because of their unusual magnetic and electrical properties, as well as for their interesting structural and dynamic characteristics (Galasso, 1969; Muller & Roy, 1974; Scott, 1974). Quite recently, the discovery of high-temperature superconductivity in perovskite phases has led to a gigantic resurgence of interest in their structure. Titanates (including the prototypical mineral perovskite, $CaTiO_3$) also form a basis for advanced ceramic nuclear waste forms while other perovskites, such as $BaPuO_3$, which contain transuranic and fission-product elements are relevant to nuclear waste immobilization processes (Ringwood,

* Computing and Communications Division.
† Author to whom correspondence should be directed at Los Alamos Neutron Scattering Center (LANSCE).
‡ Isotopes and Nuclear Chemistry Division.
§ Applied Theoretical Physics Division.
¶ Materials Science and Technology Division.

0108-7681/88/060575-06$03.00